Generic picture of the emission properties of III-nitride polariton laser diodes: Steady state and current modulation response

Ivan Iorsh
Department of Physics, Durham University, Durham DH1 3LE, United Kingdom

Marlene Glauser, Georg Rossbach, Jacques Levrat, Munise Cobet, Raphaël Butté,* and Nicolas Grandjean
Institute of Condensed Matter Physics, Ecole Polytechnique Fédérale de Lausanne (EPFL), CH-1015 Lausanne, Switzerland

Mikhail A. Kaliteevski
Saint Petersburg Academic University, St Petersburg, Russia and Ioffe Physicotechnical Institute of Russian Academy of Science, 26, Polytechnicheskaya, 194021 St-Petersburg, Russia

Richard A. Abram
Department of Physics, Durham University, Durham DH1 3LE, United Kingdom

Alexey V. Kavokin
School of Physics and Astronomy, University of Southampton, Highfield, Southampton SO17 1BJ, United Kingdom and CNRS, Charles Coulomb Laboratory, University Montpellier II, Place Eugène Bataillon, Montpellier 34095 Cedex, France
(Received 26 June 2012; published 7 September 2012)

The main emission characteristics of electrically driven polariton lasers based on planar GaN microcavities with embedded InGaN quantum wells are studied theoretically. The polariton emission dependence on pump current density is first modeled using a set of semiclassical Boltzmann equations for the exciton polaritons that are coupled to the rate equation describing the electron-hole plasma population. Two experimentally relevant pumping geometries are considered, namely the direct injection of electrons and holes into the strongly coupled microcavity region and intracavity optical pumping via an embedded light-emitting diode. The theoretical framework allows the determination of the minimum threshold current density $J_{\mathrm{thr,min}}$ as a function of lattice temperature and exciton-cavity photon detuning for the two pumping schemes. A $J_{\mathrm{thr,min}}$ value of 5 and 6 A cm^{-2} is derived for the direct injection scheme and for the intracavity optical pumping one, respectively, at room temperature at the optimum detuning. Then an approximate quasianalytical model is introduced to derive solutions for both the steady-state and high-speed current modulation. This analysis makes it possible to show that the exciton population, which acts as a reservoir for the stimulated relaxation process, gets clamped once the condensation threshold is crossed, a behavior analogous to what happens in conventional laser diodes with the carrier density above threshold. Finally, the modulation transfer function is calculated for both pumping geometries and the corresponding cutoff frequency is determined.

DOI: 10.1103/PhysRevB.86.125308 PACS number(s): 71.36.+c, 03.75.Nt, 78.67.De, 42.55.Sa

I. INTRODUCTION

In recent years, the physics of polariton condensates—systems of condensed bosonic quasiparticles resulting from the strong coupling of cavity photons and excitons in semiconductor microcavity (MC) structures[1,2]—has become one of the most flourishing fields of contemporary condensed matter physics. This can be partly attributed to the wealth of such condensates in terms of exotic physical properties that lie at the frontiers of several areas, such as nonlinear optics, laser physics, and quantum phase transitions leading to macroscopic coherent states, to cite just a few.

In the field of quantum phase transitions, research was mainly triggered by the report of the Bose-Einstein condensation of polaritons occurring in CdTe-based planar MCs at cryogenic temperatures.[3] This was soon followed by reports of effects associated with condensation, such as polariton lasing occurring at room temperature (RT) in wide band gap semiconductors (inorganic or organic) exhibiting highly stable excitons/polaritons.[4–6] Other collective polariton phenomena of interest include, e.g., (i) hints of superfluidity such as the signature of integer and half-quantized vortices[7,8] and the ballistic motion of condensates,[9,10] and (ii) spontaneous coherent oscillations between adjacent condensates that share similarities with the ac Josephson effect.[11]

One aspect of polariton condensates that has remained relatively unexplored so far deals with the realization of polariton laser diodes (LDs) able to operate at RT. As far as electrical injection is concerned, well defined electroluminescence (EL) features have already been reported[12] between cryogenic and room temperatures in GaAs-based polariton light-emitting diodes (pol-LEDs). Those structures, obviously operating in the strong coupling regime (SCR), have a design relatively close to that of their near-infrared vertical cavity surface emitting laser (VCSEL) counterparts (which are based on the same material system) operating in the weak coupling regime. However, the realization of RT GaAs-based polariton LDs is probably precluded by the value of the exciton binding energy (E_X^B) in this material system [usually less than 10 meV for the quantum wells (QWs) of

interest],[13] which is small compared to the thermal energy at 300 K. Indeed, it was previously shown that the value of E_X^B is the main limiting factor for the high-temperature observation of optical nonlinearities of polaritonic origin under resonant excitation.[14] In this connection, two of the current authors emphasized in a recent review[15] the potential of III-nitride compounds compared with organic semiconductors or ZnO as suitable candidates to realize polariton LDs that could display a threshold current density (J_{thr}) down to $\sim$10 A cm^{-2} at RT, a decrease of more than two orders of magnitude compared with that of state-of-the-art GaN-based edge-emitting LDs.[16] The reason for such a low threshold originates from the fact that the condensation process is expected to occur at medium quasiparticle densities—well before the appearance of screening and phase space filling effects that would lead to the transition of polaritons and excitons toward an electron-hole plasma—due to the low effective density of states of polaritons resulting from their very light mass near the center of the Brillouin zone.

At this stage, it is helpful to recall briefly the operating principle of polariton LDs, which differs from that of conventional semiconductor lasers. As originally described by Imamoğlu and co-workers,[17] in a polariton laser the relaxation of polaritons is governed by scattering processes stimulated by final-state occupation, and the spontaneous radiative decay of these short-lived particles (lifetime in the picosecond range) forming a condensate leads to a coherent emission of photons without requiring population inversion. As will be shown hereafter, one can describe the operation of such a laser close to threshold using coupled rate equations governing the electron-hole plasma, exciton reservoir, and polariton condensate densities in a way similar to that employed for conventional semiconductor LDs when considering the electron-hole plasma and photon densities.[18] In particular, it is possible to obtain an accurate understanding of the operation of polariton LDs, in both the continuous-wave regime and under high-speed current modulation. Our work is also motivated by the possibility to electrically manipulate spinor condensates that are characterized by unique spin-dependent properties. In particular, polariton LDs could become key elements in the burgeoning field of polariton signal processing based on the creation and control of in-plane propagating polarized polariton wave packets.[19]

In the present paper, following a description of the specific sample design requirements to achieve polariton lasing under electrical injection in planar III-nitride MC samples (Sec. II), we provide a generic description of polariton LDs. We do the latter by using a system of coupled Boltzmann equations for the exciton polaritons based on experimental parameters and scattering rates deduced from microscopic modeling to describe the evolution of the carrier densities (Sec. III A). Then above threshold those equations are reduced to a quasianalytical model based on three or just two coupled rate equations, depending on the pumping geometry, for the electron-hole plasma, exciton reservoir, and polariton condensate. In this way, we describe the steady-state regime (Sec. III B) before analyzing the response of such lasers when subjected to high-speed current modulation (Sec. III C). Finally, the main conclusions are summarized (Sec. IV).

II. DESIGN OF III-NITRIDE POLARITON LASER DIODES

To begin, it is necessary to recall some aspects of III-nitride structures relevant to the implementation of an electrical injection scheme suitable for polariton LDs.[15] Recently, a theoretical study reported on the characteristics of a bulk GaN polariton LD, which predicts a J_{thr} value of $\sim$50 A cm^{-2} at RT, thereby indicating the potential of such devices as low threshold coherent light emitters.[20] Though such a structure has the advantage of simplicity, it should be noted that a realistic design for RT operation will likely rely on a multiple QW (MQW) active region because of the improved carrier confinement and the higher exciton binding energy over bulk in such two-dimensional heterostructures.

First, it should be noted that the number of quantum wells (N_{QW}) should be large enough to achieve a well defined SCR signature at RT, i.e., to get a sufficiently large normal mode splitting (Ω_{VRS}) to polariton linewidth ratio.[21] This is due to the detrimental impact of the inhomogeneous linewidth broadening of III-nitride QWs, which can blur the signature of polaritons if it is too large for a small N_{QW} value (note also that the homogeneous broadening is usually non-negligible at 300 K).[22] Then to get efficient electrical injection, the most appropriate choice of active region would be obtained by switching from the usual GaN/AlGaN MQW system to InGaN/GaN MQWs,[5,23] since obtaining good p-type conductivity becomes progressively more difficult when increasing the Al content of the AlGaN layers due to the significant rise of the activation energy of the deep Mg acceptor level.[24] At first glance, InGaN/GaN MQWs could seem to be an unpromising choice for SCR applications because of their large inhomogeneous QW linewidth. However, low indium content ($7\% < x < 10\%$) $\mathrm{In}_x\mathrm{Ga}_{1-x}\mathrm{N}$/GaN MQW MC structures with a design close to that of GaN/AlGaN MQW MC samples[5,21] are expected to exhibit clear SCR features and polariton lasing under optical pumping at RT. This approach is also motivated by the recent development of crack-free, lattice-matched AlInN/GaN distributed Bragg reflectors (DBRs) grown on free-standing GaN substrates that combine low dislocation density ($\leqslant 10^6$ cm^{-2}), smooth rms surface roughness ($\sim$0.26 nm for a 4×4 μm^2 area), and high peak reflectivity ($R \sim 99.6\%$).[25] Microcavity structures grown on such a DBR would certainly exhibit a much improved optical quality, i.e., a reduced in-plane cavity disorder compared with similar structures grown on c-plane sapphire substrates.[26]

With such MC samples, another matter to be addressed is the achievement of a uniform injection of electrons and holes in the active region, which is known to be an issue in III-nitride optoelectronic devices.[27] A way to circumvent the conflicting requirements presented by a structure where N_{QW} should be large for SCR purposes and small for electrical injection would be to use an intracavity pumping geometry (Fig. 1).[28] Within such a pumping scheme, a small number of QWs sandwiched in the intrinsic region of a p-i-n diode would be electrically pumped. This QW subset (QWs-1), *a priori* not taking part in the formation of polaritons, would emit photons at an energy greater than the absorption edge of a MQW region (second QW subset, QWs-2) located underneath and which would be in the SCR so that QWs-1 could act as an efficient internal pump for the generation of polaritons. Other specific

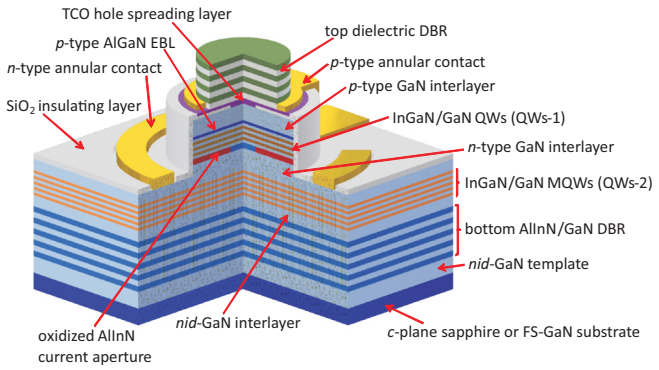

FIG. 1. (Color online) Schematic 3D cross section of an InGaN/GaN MQW polariton LD based on an intracavity pumping geometry.

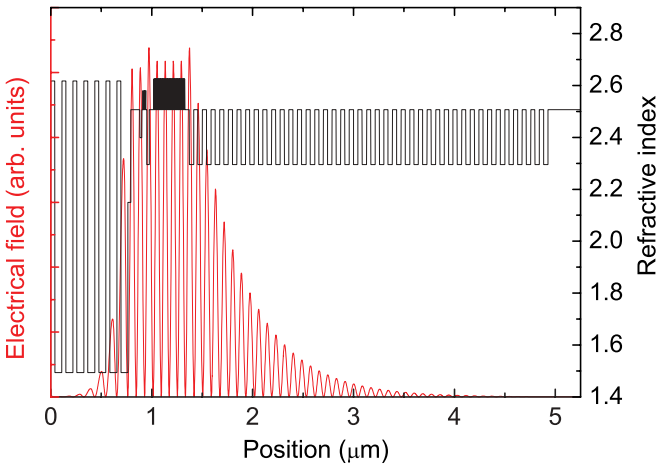

FIG. 2. (Color online) Results of a transfer matrix simulation of the field intensity profile of a polariton LD centered at $\lambda = 415$ nm along with the corresponding refractive index profile.

constraints regarding the design of polariton LDs have been described in Ref. 15 and are included in the three-dimensional (3D) cross section of the InGaN/GaN MQW polariton LD displayed in Fig. 1. An intracavity contact scheme is used, as has already been discussed in the case of III-nitride VCSEL structures.[29] To compensate for the relatively poor lateral hole spreading into the p-type GaN layer, which is mainly due to current crowding—a detrimental effect whose impact is enhanced by the annular contact geometry—and thus to get light emission from the active region sandwiched between the DBRs, various approaches can be implemented. First, a buried oxidized AlInN interlayer can be inserted on the n-side underneath QWs-1 in a similar fashion to that implemented for micro-LEDs[30] to confine the electron current flow in the central part of the device. A transparent conductive oxide (TCO), such as indium tin oxide or ZnO, sandwiched between the p-type GaN layer and the top dielectric DBR[31] (cf. Fig. 1) also appears well suited to improve the lateral spreading of the hole current. Then the use of an electron-blocking layer (EBL) located on top of the electrically pumped region is intended to avoid an excess of electrons on the p-type side and thus limit unwanted electron-hole recombination.[32]

Beyond issues related to electrical pumping, another critical parameter when considering the above-mentioned geometry is the significant increase in the effective cavity length (L_{eff}). Indeed, it is known that as a first approximation, Ω_{VRS} scales like $1/\sqrt{L_{\text{eff}}}$.[33] However, L_{eff} also accounts for the penetration depth of the electromagnetic field into the DBRs, and one way to compensate for its unavoidable increase is to use a top dielectric DBR with a short penetration depth. This can be achieved by adopting the SiO_2/TiO_2 bilayer system since it exhibits a very large refractive index contrast [$n_{TiO_2}(\lambda = 415\text{ nm}) = 2.6$ versus $n_{SiO_2}(\lambda = 415\text{ nm}) = 1.495$].[15] As an illustration, the penetration depth obtained at $\lambda = 415$ nm only amounts to $0.83\lambda/2$ for a SiO_2/TiO_2 DBR against $2.47\lambda/2$ for the more conventional SiO_2/Si_3N_4 structure, where $n_{Si_3N_4}(\lambda = 415\text{ nm}) = 1.83$.[34–36] Note, however, that the former type of DBR is not suited for a nonresonant optical pumping geometry due to the strong rise in the absorption occurring in TiO_2 layers for wavelengths shorter than 375 nm. The electric field profile of the complete structure, derived from transfer matrix simulation, along with the corresponding refractive index profile are displayed in Fig. 2 at $\lambda = 415$ nm. Refractive indices for the III-nitride compounds were taken from the work of Brunner *et al.*[37] (AlGaN alloys), Carlin *et al.*[38,39] (AlInN alloys), and Bergmann and Casey[40] (InGaN alloys), respectively, and the refractive index value for ZnO was taken from the work of Schmidt *et al.*.[41]

III. FORMALISM

A. Coupled semiclassical Boltzmann equations for an electrically driven exciton-polariton device

To predict the main characteristics of polariton LDs, we first consider a kinetic model based on a set of coupled semiclassical Boltzmann equations for exciton polaritons, in which all polariton states within the light cone are accounted for. To better illustrate the particular properties of the polariton LD based on intracavity optical pumping that was introduced in the previous section, two pumping schemes are considered. In the first scheme, it is assumed that electrically pumped electrons and holes are uniformly injected into the set of strongly coupled QWs, emitting at ~415 nm (i.e., the QW subset QWs-1 is ignored). Such a scheme is not well suited to III-nitride structures with a large N_{QW} but it is adopted as a simplified approach, and one that is potentially applicable to low-temperature GaAs-based polariton LDs. After some time, charge carriers are either removed due to nonradiative recombination occurring at dislocations, trapping, or Auger recombination, or they bind into pairs forming excitons. Those excitons may be characterized by various energies and in-plane wave vectors (k) and their ensemble is described as an incoherent reservoir pumped from the electron-hole plasma. This exciton reservoir then feeds the condensate of exciton polaritons, which is a coherent multiparticle state responsible for polariton lasing.

The second scheme concerns the design shown in Fig. 1, where the region QWs-1, ideally emitting in the 390–400 nm range, is uniformly electrically pumped by charge carriers, and high-energy photons subsequently emitted by those QWs are then absorbed by QWs-2,[15] which is the set of strongly coupled QWs, that will lead to the formation of an incoherent exciton reservoir. This intracavity optical pumping geometry

essentially differs from the first one due to the following reasons: (i) Overall, for a given current density, the population of excitons in the reservoir feeding the condensate will be smaller due to the internal quantum efficiency (IQE), which is less than 100%. This latter quantity is taken to be 90%, which corresponds to that of state-of-the-art LEDs. (ii) The density of free carriers in the region QWs-2 is constant since they are located in the n-type region (cf. Fig. 1), whereas this density is current-dependent in the previous injection scheme and will have an impact on the injection dependence of the exciton–free-carrier scattering term. (iii) While one can assume that in the intracavity optical pumping scheme, free electrons in the n-doped region are thermalized and obey Fermi statistics with an effective temperature (T_{eff}) close to the lattice temperature (T_{latt}), in the direct electrical pumping scheme electrons are not thermalized with the lattice. In this latter situation, we consider a Boltzmann carrier distribution with $T_{\text{eff}} > T_{\text{latt}}$.

We include in the model three possible mechanisms of exciton(-polariton) scattering into the condensate: phonon scattering (acoustic-phonon assisted scattering, which consists of the deformation potential and piezoelectric terms, and LO-phonon assisted scattering mediated by the Fröhlich interaction), exciton(-polariton)-exciton(-polariton) scattering, and exciton(-polariton)–free carrier scattering. Note that this last scattering term should *a priori* differ significantly between the two pumping schemes due to the different free carrier distributions considered in each case. Besides this, the radiative recombination of excitons lying at higher k states, which do not contribute to polariton lasing, is also taken into account by introducing the exciton radiative lifetime. The depletion of the polariton condensate occurs both through spontaneous radiative recombination and by the absorption of acoustic phonons, which brings exciton polaritons back to k states beyond the inflection point of the lower polariton branch (LPB).[42,43] We neglect other mechanisms of depletion of the condensate (e.g., due to polariton-polariton scattering) assuming they are less probable.

All the above-mentioned processes are described by the following set of rate equations:

$$\frac{dn_k}{dt} = P_k - \frac{n_k}{\tau_k} + \sum_{k' \neq k} [W_{k'k} n_{k'}(n_k + 1) - W_{kk'} n_k (n_{k'} + 1)]. \tag{1}$$

Here n_k is the concentration of exciton polaritons with in-plane wave vector k, and P_k describes the electronic pumping rate. τ_k is the polariton radiative lifetime, $W_{kk'}$ is the total scattering rate between quantum states indicated by k and k' with $k = (k_x, k_y)$, $k_{x,y} = \pm 2\pi j/L$, $j = 0,1,2,\ldots,$ and $|k| < \omega/c$, where L is the lateral size of the system, ω is the frequency of the exciton resonance, and c is the speed of light.

We first consider the direct electrical pumping geometry. For the sake of simplicity, it is convenient to define the pumping as a function of the energy along the lower polariton branch E_k:

$$P_k = 0 \tag{2}$$

if $E_k - E_X < \Delta$, and

$$P_k = \frac{W n_{e\text{-}h}}{\widetilde{N}} \tag{3}$$

if $E_k - E_X \geqslant \Delta$, where E_X is the exciton energy at the center of the first Brillouin zone and $\Delta = 45$ meV is the exciton binding energy deduced from the variational approach developed by Leavitt and Little.[21,44] W is the exciton formation rate from the electron-hole plasma, $\widetilde{N}$ is the number of states within the light cone which satisfy the condition $E_k \geqslant E_X + \Delta$, and $n_{e\text{-}h}$ is the concentration of electron-hole pairs, which is given by

$$\frac{dn_{e\text{-}h}}{dt} = \frac{J}{q} - \frac{n_{e\text{-}h}}{\tau_{e\text{-}h}} - W n_{e\text{-}h}, \tag{4}$$

where J is the electric pumping rate, q is the elementary charge, and $\tau_{e\text{-}h}$ is the decay rate of the electron-hole plasma.

Equation (4) can be solved analytically to yield a simple dependence:

$$n_{e\text{-}h}(t) = \frac{J}{q} \frac{\tau_{e\text{-}h}}{1 + W\tau_{e\text{-}h}} \left[1 - \exp\left(-Wt - \frac{t}{\tau_{e\text{-}h}}\right)\right], \tag{5}$$

assuming an electron-hole plasma density equal to zero at $t = 0$.

For the intracavity optical pumping geometry, we consider that strongly coupled quantum wells are indirectly optically pumped with an energy-dependent pump intensity given by

$$P_k = \frac{\eta_{\text{int}} J}{\sqrt{2\pi}(\delta E)} \exp\left(-\frac{(E_k - E_{\text{pump}})^2}{2(\delta E)^2}\right). \tag{6}$$

Here η_{int} is the internal quantum efficiency of the pumping LED,[45] E_{pump} is the central energy of the LED, which is set equal to the exciton energy of QWs-1, and δE is the linewidth of the LED, which is set to 90 meV and is considered temperature-independent as a first approximation.[46] Note here that for the sake of illustration, we consider the limiting case in which the pumping QW set (QWs-1) is resonant with the exciton energy of the second QW set (QWs-2), which leads to the formation of polaritons, to make a clear distinction between the two possible pumping geometries. However, in the more general case, a nonresonant intracavity pumping scheme would likely apply.

The scattering rates $W_{kk'}$ are decomposed as

$$W_{kk'} = W_{kk'}^{\text{phon}} + W_{kk'}^{\text{el}} + W_{kk'}^{\text{pol-pol}}, \tag{7}$$

where $W_{kk'}^{\text{phon}}$ is the combination of acoustic-phonon and LO-phonon assisted scattering rates, $W_{kk'}^{\text{el}}$ is the scattering rate assisted by free electrons or holes, and $W_{kk'}^{\text{pol-pol}}$ is the polariton-polariton scattering rate. We obtain these rates using the formalism developed in Ref. 47.

Note that the model we use differs from the system of rate equations proposed by Tassone and Yamamoto to describe optically pumped microcavities in the polariton lasing regime.[48] In particular, it explicitly accounts for the electron-hole plasma and introduces the exciton-electron scattering as one of the important mechanisms of exciton(-polariton) relaxation into the condensate.

In the numerical calculations, we have used the following set of parameters: τ_k is calculated assuming a cavity photon lifetime $\tau_{\text{cav}} = 1$ ps and an exciton lifetime $\tau_x = 1$ ns.[49] The lateral size of the system was taken equal to $L = 50$ μm, $\tau_{e\text{-}h} = 5$ ns,[50] and $W = 0.01$ ps^{-1}. When calculating the matrix elements $W_{kk'}$, we have also considered an exciton binding energy of 45 meV, a normal mode splitting of

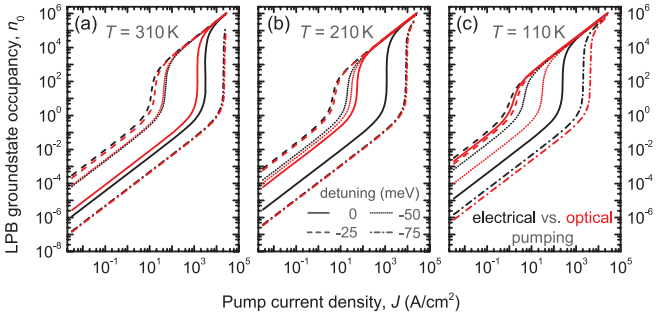

FIG. 3. (Color online) (a)–(c) Occupancy of the polariton ground state vs pump current density calculated for the two pumping geometries at various temperatures and detunings (see text for details).

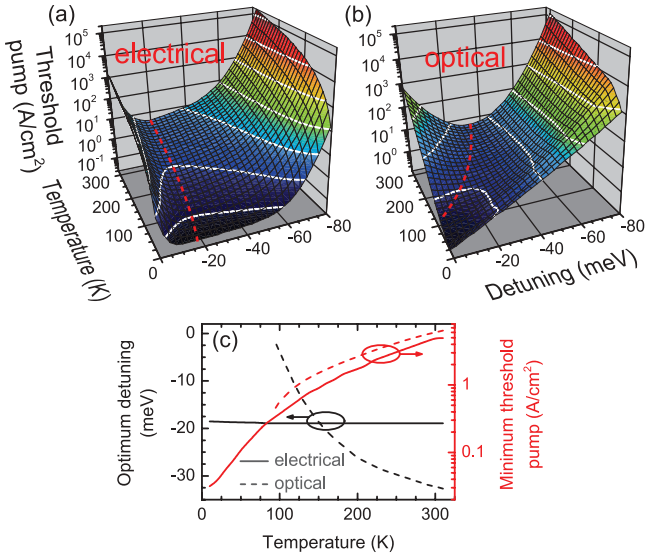

FIG. 4. (Color online) Plots of $J_{\rm thr}$ vs detuning and temperature for (a) the direct electrical and (b) the intracavity optical pumping schemes. The red dashed line in each plot corresponds to the evolution of $J_{\rm thr,min}$ as a function of temperature. (c) Evolution of the optimum detuning (black solid and black dashed lines) and condensation threshold current density (red solid and red dashed lines) at the optimum detuning as a function of lattice temperature for the direct electrical (solid lines) and the intracavity (dashed lines) pumping schemes.

45 meV, deduced from transfer matrix simulations, a number of QWs $N_{\rm QW} = 65$, an exciton inhomogeneous line broadening $\gamma_{\rm ex} = 45$ meV, effective electron and hole masses equal to $m_e = 0.2m_0$ and $m_h = 1.1m_0$, respectively,[51] where m_0 is the free-electron mass, a bulk exciton Bohr radius $a_B = 3.2$ nm, an effective refractive index $n = 2.6$, an LO-phonon energy $E_{\rm LO} = 92$ meV, a deformation potential $D = 11.1$ eV,[52] a mass density $\rho = 6150$ kg/m^3, and a speed of sound (in the [0001] direction) $c_s = 7960$ m/s.[53] These parameters correspond to what we expect for state-of-the-art GaN-based microcavities with embedded InGaN/GaN quantum wells. The internal quantum efficiency of the pumping LED in the case of intracavity pumping was set to 0.9 and the effective electron temperature in the case of direct electrical pumping was set to 800 K.

Figure 3 shows the evolution of the ground state polariton occupation number versus pump current density for different temperatures and detunings for the two pumping geometries. The threshold current density for condensation ($J_{\rm thr}$) can be clearly identified in each case.

We have also displayed the $J_{\rm thr}$ dependence as a function of temperature and detuning in Fig. 4. In this way, one obtains the polariton condensation phase diagram under electrical pumping, which is analogous to that derived under optical pumping for GaN/AlGaN MQW MCs.[23,43] One can see that at room temperature, the lowest threshold current density ($J_{\rm thr,min}$) is obtained for a negative detuning of -19 meV and amounts to $\sim$5 A cm^{-2} for the direct electrical pumping geometry, while a $J_{\rm thr,min}$ value of $\sim$6 A cm^{-2} at a negative detuning of -32 meV is derived for the intracavity pumping geometry. Those values are in good agreement with that predicted in previous work.[15,16] This optimum detuning ($\delta_{\rm opt}$) corresponds to the case in which the mean polariton relaxation time equals the mean polariton lifetime.[43,54] The system then switches from the kinetic to the thermodynamic regime. In other words, it undergoes a crossover from a regime where $J_{\rm thr}$ decreases with increasing detuning (decreasing δ in absolute value) because of the enhancement of the total scattering rate to the ground state, to a regime where $J_{\rm thr}$ increases concomitantly with δ due to the combined effects of the increasing polariton effective mass (which leads to a larger value of the critical density for polariton condensation, $n_{\rm 2D,crit}$) and thermal detrapping from the ground state.[43] It is also noticeable that the temperature dependence of $\delta_{\rm opt}$ significantly differs from one geometry to the other [Figs. 4(a)–4(c)]. This is attributed to the difference in the efficiency of the free electron scattering mechanism as a function of temperature.[55] For the direct electrical pumping geometry, the electron distribution does not depend on $T_{\rm latt}$ since electrons are not thermalized, thus leading only to slight changes in the free electron scattering rate with temperature and thereby explaining the weak $\delta_{\rm opt}(T)$ variation displayed in Figs. 4(a) and 4(c). For the intracavity optical pumping geometry, electrons are thermalized to $T_{\rm latt}$, which leads to a behavior closer to that reported for GaN/AlGaN MQW MCs under nonresonant optical pumping [Figs. 4(b) and 4(c)].[43] However, it should be recognized that assuming an electron temperature equal to $T_{\rm latt}$ is a crude approximation. We should also point out that, for the sake of simplicity, we did not account for the large activation energy of the Mg acceptor in GaN compounds, which would most likely degrade the electrical characteristics and thus lead to an increase in $J_{\rm thr}$ at low temperatures.

The low threshold values reported for the intracavity pumping geometry can probably be explained by the broad spectral distribution of the pump P_k. In the direct electrical injection geometry, excitons characterized by high energies and large in-plane wave vectors are created from the electron-hole plasma, which requires a comparatively long time to relax to the $k = 0$ state. However, in the case of intracavity optical pumping, a broad distribution of excitons centered on the QW-1 exciton energy, but also covering lower energy states, is created. Those excitons which occupy lower energy and lower k states compared with the direct electrical pumping geometry quickly relax to the lower polariton branch ground

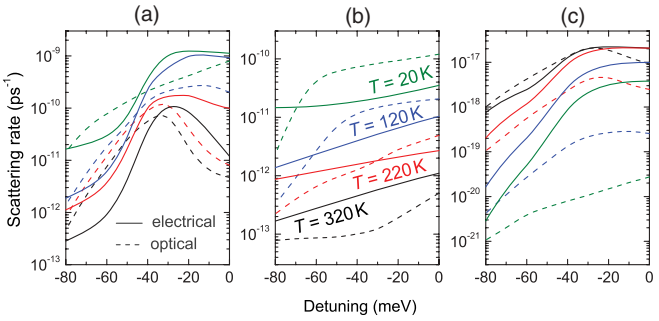

FIG. 5. (Color online) Averaged scattering rates a, b, and c as a function of detuning obtained by fitting the full semiclassical Boltzmann system of equations at various temperatures for the two pumping schemes: electrical (solid lines) and intracavity (dashed lines) pumping.

state and enhance polariton relaxation, which results in the lower threshold for this geometry. However, if the intracavity emission line is strongly blueshifted from the polariton modes, the ratio between the polariton lasing thresholds for the two pumping configurations is expected to be modified. One would then expect a higher threshold for the intracavity pumping geometry due to the IQE of the internal pump, which is less than 100%.

B. Simplified rate equation modeling: Steady-state solutions

To obtain a qualitative understanding of the functionality of polariton laser diodes, we compare the modeling results obtained with the full set of semiclassical Boltzmann equations with a simplified quasianalytical model. For the direct electrical pumping geometry, the model is based on three rate equations describing the electron-hole plasma [namely Eq. (4) introduced in Sec. III A], the exciton reservoir, and ground state polaritons, respectively:

$$\frac{dn_x}{dt} = -\frac{n_x}{\tau_x} + Wn_{e\text{-}h} - an_x(n_p+1) + ae^{-\beta\Delta_{\rm esc}}n_pn_x - bn_x^2(n_p+1) - cn_{e\text{-}h}n_x(n_p+1), \tag{8}$$

$$\frac{dn_p}{dt} = -\frac{n_p}{\tau_p} + an_x(n_p+1) - ae^{-\beta\Delta_{\rm esc}}n_pn_x + bn_x^2(n_p+1) + cn_{e\text{-}h}n_x(n_p+1), \tag{9}$$

where n_x and n_p are the concentrations of excitons and exciton polaritons, respectively. τ_p is the lifetime of exciton polaritons in the ground state. a accounts for the acoustic and optical phonon relaxation rates, $\beta = 1/k_BT$, and $\Delta_{\rm esc}$ is the characteristic energy splitting between the bottom of the LPB and states beyond the inflection point of the LPB where zero in-plane wave-vector polaritons are scattered, which is a quantity sensitive to the detuning.[23,42,43] b is the exciton-exciton scattering rate and c is the rate of exciton relaxation mediated by free carriers. The solid curves in Fig. 5 show the detuning dependence of the fitting parameters a, b, and c (for different temperatures) for them to yield the same threshold pumping current density for the direct electrical pumping scheme as the full semiclassical Boltzmann model (considered as a reference).

If now the more realistic intracavity optical pumping geometry is considered, the previous quasianalytical three-level model can be simplified further to a two-level model since the free carrier dynamics does not have to be accounted for explicitly. Then

$$\frac{dn_x}{dt} = P_x - \frac{n_x}{\tau_x} - an_x(n_p+1) + ae^{-\beta\Delta_{\rm esc}}n_pn_x - bn_x^2(n_p+1) - cn_dn_x(n_p+1), \tag{10}$$

$$\frac{dn_p}{dt} = -\frac{n_p}{\tau_p} + an_x(n_p+1) - ae^{-\beta\Delta_{\rm esc}}n_pn_x + bn_x^2(n_p+1) + cn_dn_x(n_p+1), \tag{11}$$

where n_d is the concentration of free carriers obtained from the doping level in the region QWs-2, and taken equal to 2×10^{12} cm^{-2}. In the simplest approximation, P_x can be taken to be $P_x = \eta_{\rm int}J/q$, where $\eta_{\rm int}$ is the IQE of the electrically pumped region QWs-1. The dashed lines in Fig. 5 show the values of the fitting parameters a, b, and c which yield the same threshold pumping current density for the intracavity optical pumping scheme as the full semiclassical Boltzmann model for different temperatures and detunings.

One can see in this latter figure that—overall—all the scattering mechanisms that contribute to populate the polariton lasing mode become more efficient with decreasing negative detuning (in absolute value). It stems from the reduced exciton fraction of polariton states at large negative detuning, so that all interactions involving polaritons become weaker than at zero or positive detuning. In some cases, the detuning dependence of the scattering rates is nonmonotonic and it is also sensitive to the pumping scheme. This is due to the complexity of the lower polariton branch dispersion. The average scattering rates are therefore sensitive to both the shape of the polariton dispersion and the excitation spectrum profile.

Above threshold, the $(1+n_p)$ and $(1+n_x)$ terms appearing in the rate equations can be approximated as n_p and n_x, respectively. After some algebra, the steady-state solutions ($t=+\infty$) for the electron-hole pair, exciton, and polariton populations for the direct electrical pumping geometry are obtained as

$$n_{e\text{-}h_\infty} = \frac{J\tau_{e\text{-}h}}{q(1+\tau_{e\text{-}h}W)}, \tag{12}$$

$$n_{x_\infty} = \frac{-cn_{e\text{-}h_\infty} + a(e^{-\beta\Delta_{\rm esc}}-1) + \sqrt{[-cn_{e\text{-}h_\infty} + a(e^{-\beta\Delta_{\rm esc}}-1)]^2 + \frac{4b}{\tau_p}}}{2b}, \tag{13}$$

$$n_{p_\infty} = \tau_p\left(Wn_{e\text{-}h_\infty} - \frac{n_{x_\infty}}{\tau_x}\right). \tag{14}$$

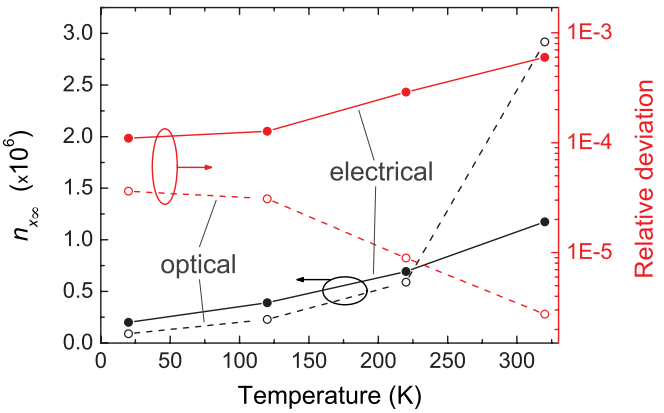

FIG. 6. (Color online) Left-hand side vertical scale: evolution of n_{x_∞} as a function of temperature calculated at the optimum detuning using the exact expressions for the electrical (connected black dots) and the intracavity (connected black circles) pumping geometries (see text for details). Right-hand side vertical scale: relative deviation between the exact and the approximated expressions for the electrical (connected red dots) and the intracavity (connected red circles) pumping geometries.

Note that for the intracavity optical pumping geometry, slight changes occur since $n_{e\text{-}h_\infty}$ in Eq. (13) has to be replaced by n_d, and $Wn_{e\text{-}h_\infty}$ in Eq. (14) has to be replaced by P_x. We should emphasize that for this latter geometry, the carrier population, which acts as a reservoir for the stimulated relaxation process (here the excitons), gets clamped once it crosses the condensation threshold, which is expected due to the similarities of the above-mentioned rate equations with those describing conventional laser diodes.[18] A similar treatment can be used for the direct electrical pumping geometry since $4b/\tau_p \gg [-cn_{e\text{-}h_\infty} + a(e^{-\beta\Delta_{\rm esc}} - 1)]^2$. Thus, for both cases, we obtain $n_{x_\infty} \approx 1/\sqrt{b\tau_p}$. The evolution of n_{x_∞} as a function of temperature at the optimum detuning is shown in Fig. 6 using both the exact expression and the approximate one for the two pumping geometries. The validity of the approximation for n_{x_∞} is confirmed by the close correspondence between the two quantities independent of the temperature. Considering its approximate expression, the increase with temperature of n_{x_∞} can be directly inferred from the results displayed in Fig. 5, which show a decrease in the exciton-exciton scattering rate b with increasing $T_{\rm latt}$, and it is also fully consistent with the overall temperature dependence of the analytical expression for b derived by Tassone and Yamamoto.[48] Note that one also expects a decrease in n_{x_∞} with increasing detuning[56] likely due to the concomitant increase in the relaxation process from the excitonic reservoir (which coincides with the decrease or even the disappearance of the relaxation bottleneck) and that of τ_p.[48]

C. Simplified rate equation modeling: High-speed current modulation treatment

In this section, the dynamical response of polariton LDs to a small perturbation, such as a modulation of the current above threshold, is investigated. Since exact analytical solutions to the full rate equations cannot be obtained, a differential analysis of the simplified rate equations given in the previous section using the approach described by Coldren and Corzine for the case of conventional LDs is considered.[57,58] The resulting small-signal responses are derived by taking the differential of the rate equations which can be written in compact matrix form for the two pumping geometries as follows:

Electrical pumping geometry:

$$\frac{d}{dt}\begin{bmatrix} dn_x \\ dn_p \end{bmatrix} = \begin{bmatrix} -\gamma_{xx} & -\gamma_{xp} \\ \gamma_{px} & -\gamma_{pp} \end{bmatrix}\begin{bmatrix} dn_x \\ dn_p \end{bmatrix} + \begin{bmatrix} dn_{e\text{-}h}(W - cn_{x_\infty}n_{p_\infty}) \\ 0 \end{bmatrix}, \quad (15)$$

where

$$\gamma_{xx} = \frac{1}{\tau_x} + an_{p_\infty} + 2bn_{x_\infty}n_{p_\infty} + cn_{e\text{-}h_\infty}n_{p_\infty} - an_{p_\infty}e^{-\beta\Delta_{\rm esc}}, \quad (16)$$

$$\gamma_{pp} = \frac{1}{\tau_p} - an_{x_\infty} - bn_{x_\infty}^2 - cn_{e\text{-}h_\infty}n_{x_\infty} + an_{x_\infty}e^{-\beta\Delta_{\rm esc}}, \quad (17)$$

$$\gamma_{xp} = an_{x_\infty} + bn_{x_\infty}^2 + cn_{e\text{-}h_\infty}n_{x_\infty} - an_{x_\infty}e^{-\beta\Delta_{\rm esc}}, \quad (18)$$

$$\gamma_{px} = an_{p_\infty} + 2bn_{x_\infty}n_{p_\infty} + cn_{e\text{-}h_\infty}n_{p_\infty} - an_{p_\infty}e^{-\beta\Delta_{\rm esc}}. \quad (19)$$

Intracavity pumping geometry:

$$\frac{d}{dt}\begin{bmatrix} dn_x \\ dn_p \end{bmatrix} = \begin{bmatrix} -\gamma_{xx} & -\gamma_{xp} \\ \gamma_{px} & -\gamma_{pp} \end{bmatrix}\begin{bmatrix} dn_x \\ dn_p \end{bmatrix} + \begin{bmatrix} \frac{\eta_{\rm int}}{q}dJ \\ 0 \end{bmatrix}, \quad (20)$$

where

$$\gamma_{xx} = \frac{1}{\tau_x} + an_{p_\infty} + 2bn_{x_\infty}n_{p_\infty} + cn_dn_{p_\infty} - an_{p_\infty}e^{-\beta\Delta_{\rm esc}}, \quad (21)$$

$$\gamma_{pp} = \frac{1}{\tau_p} - an_{x_\infty} - bn_{x_\infty}^2 - cn_dn_{x_\infty} + an_{x_\infty}e^{-\beta\Delta_{\rm esc}}, \quad (22)$$

$$\gamma_{xp} = an_{x_\infty} + bn_{x_\infty}^2 + cn_dn_{x_\infty} - an_{x_\infty}e^{-\beta\Delta_{\rm esc}}, \quad (23)$$

$$\gamma_{px} = an_{p_\infty} + 2bn_{x_\infty}n_{p_\infty} + cn_dn_{p_\infty} - an_{p_\infty}e^{-\beta\Delta_{\rm esc}}. \quad (24)$$

To obtain the small-signal response of the exciton (dn_x) and the polariton (dn_p) populations to a sinusoidal current modulation dJ, we assume solutions of the form $dJ = J_1\exp(i\omega t)$, $dn_{e\text{-}h} = n_{e\text{-}h1}\exp(i\omega t)$, $dn_x = n_{x1}\exp(i\omega t)$, and $dn_p = n_{p1}\exp(i\omega t)$. The linear systems (15) and (20) can then be solved for the small-signal polariton population by simply applying Cramer's rule. The small-signal solutions after expansion of the determinants can be written as follows:

Electrical pumping geometry:

$$n_{p1}(\omega) = \frac{\gamma_{px}[W - cn_{x_\infty}n_{p_\infty}] + (i\omega + \gamma_{xx})cn_{x_\infty}n_{p_\infty}}{(\gamma_{px}/\tau_p - \omega^2 + i\omega\gamma_{xx})} \times \frac{J_1/q}{i\omega + W + 1/\tau_{e\text{-}h}} = n_{p1}(0)H(\omega), \quad (25)$$

where $H(\omega)$ is the modulation transfer function given by

$$H(\omega) = \frac{\gamma_{px}/\tau_p(W + 1/\tau_{e\text{-}h})}{\gamma_{px}[W - cn_{x_\infty}n_{p_\infty}] + \gamma_{xx}cn_{x_\infty}n_{p_\infty}} \times \frac{\gamma_{px}\left[W - cn_{x_\infty}n_{p_\infty}\right] + (i\omega + \gamma_{xx})cn_{x_\infty}n_{p_\infty}}{(\gamma_{px}/\tau_p - \omega^2 + i\omega\gamma_{xx})(i\omega + 1/\tau_{e\text{-}h} + W)}. \quad (26)$$

Intracavity pumping geometry:

$$n_{p1}(\omega) = \frac{\gamma_{px}\eta_{\text{int}}J_1/q}{(\gamma_{px}/\tau_p - \omega^2 + i\omega\gamma_{xx})} = n_{p1}(0)H(\omega), \quad (27)$$

where $H(\omega)$ is the modulation transfer function given by

$$H(\omega) = \frac{\gamma_{px}/\tau_p}{(\gamma_{px}/\tau_p - \omega^2 + i\omega\gamma_{xx})}. \quad (28)$$

For both pumping geometries, a relaxation resonance frequency equal to $\omega_{R,\text{polLD}} = \sqrt{\gamma_{px}/\tau_p}$ can be defined while the γ_{xx} term can be readily identified with a damping factor.

The expression for γ_{px} derived for the two geometries [Eqs. (19) and (24)] can be greatly simplified since the term describing the exciton-exciton interaction ($\propto b$) dominates over the phonon-exciton and the free-carrier–exciton scattering terms ($\propto a$ and c, respectively) independent of the exciton-photon detuning and the temperature (cf. Fig. 6 and corresponding comments in Sec. III B). Consequently, the square of the resonance frequency reduces to

$$\omega^2_{R,\text{polLD}} \approx \frac{2bn_{x_\infty}n_{p_\infty}}{\tau_p} \approx 2n_{p_\infty}\sqrt{\frac{b}{\tau_p^3}}. \quad (29)$$

Therefore, within this theoretical framework, the resonance frequency for polariton LDs is directly proportional to the square root of the polariton population in the condensate and inversely proportional to the square root of the polariton lifetime (keeping in mind that the exciton population of the reservoir n_{x_∞} is clamped above threshold). In this respect, such a dependence is similar to the dependence of ω_R in conventional LDs above threshold, since in this latter case,

$$\omega_R^2 \approx \frac{v_g a_{\text{diff}} N_p}{\tau_{\text{cav}}}, \quad (30)$$

where v_g is the group velocity, a_{diff} is the differential gain, N_p is the average photon density in the cavity, and τ_{cav} is the cavity photon lifetime already defined in Sec. III A.[57]

From Eqs. (16) and (21), the damping factor can be rewritten as

$$\gamma_{xx} = \frac{1}{\tau_x} + \gamma_{px} = \frac{1}{\tau_x} + \omega_R^2\tau_p. \quad (31)$$

It is thus seen that for large resonance frequencies, the damping of the response is ruled by the polariton lifetime. On the other hand, the inverse of the exciton lifetime acts as a damping factor offset, which is important for small polariton condensate populations where the resonance frequency is small.

At this stage, we should point out that the validity of the previous treatment for the intracavity pumping scheme might be limited by the actual response of the pumping LED. Therefore, it is necessary to determine the LED cutoff frequency $\omega_{3\text{ dB,LED}}$, i.e., the frequency at which the electrical power response drops to half its dc value, and compare it to $\omega_{R,\text{polLD}}$.

Following the theoretical approach described in the previous sections, the rate equations governing the emission of the LED are given by Eq. (4) and

$$\frac{dn_x}{dt} = -\frac{n_x}{\tau_x} + Wn_{e\text{-}h} \quad (32)$$

(Ref. 59), from which one can deduce the modulation transfer function $H_{\text{LED}}(\omega)$ using harmonic analysis:

$$H_{\text{LED}}(\omega) = \frac{\frac{1}{\tau_x}\left(\frac{1}{\tau_{e\text{-}h}} + W\right)}{\left(i\omega + \frac{1}{\tau_x}\right)\left(i\omega + \frac{1}{\tau_{e\text{-}h}} + W\right)}. \quad (33)$$

The corresponding relaxation resonance frequency $\omega_{R,\text{LED}}$ and the damping factor γ_{LED} can be written as

$$\omega_{R,\text{LED}} = \sqrt{\frac{1}{\tau_x}\left(\frac{1}{\tau_{e\text{-}h}} + W\right)} \approx 3.2\text{ GHz} \quad (34)$$

and

$$\gamma_{\text{LED}} = \frac{1}{\tau_x} + \frac{1}{\tau_{e\text{-}h}} + W = 11.2\text{ GHz}, \quad (35)$$

respectively.

Additional features of the LED response can be derived from the frequency dependence of the square modulus of $H_{\text{LED}}(\omega)$. On a general basis, such a response is characterized by a second-order, low-pass-band filter behavior with a damped resonance appearing near the cutoff frequency $\omega_{\text{LED},3\text{ dB}}$. For $|H_{\text{LED}}(\omega)|^2$, the expression for the peak frequency of the resonance $\omega_{P,\text{LED}}$ is given by

$$\omega^2_{P,\text{LED}} = \omega^2_{R,\text{LED}}\left[1 - \frac{1}{2}\left(\frac{\gamma_{\text{LED}}}{\omega_{R,\text{LED}}}\right)^2\right], \quad (36)$$

and that of the cutoff frequency $\omega_{\text{LED},3\text{ dB}}$ is given by

$$\omega^2_{3\text{ dB,LED}} = \omega^2_{P,\text{LED}} + \sqrt{\omega^4_{P,\text{LED}} + \omega^4_{R,\text{LED}}}. \quad (37)$$

In the present case, since $\gamma_{\text{LED}} > \omega_{R,\text{LED}}$, the two previous equations reduce to

$$\omega_{P,\text{LED}} = 0 \quad (38)$$

and

$$\omega_{3\text{ dB,LED}} = \omega_{R,\text{LED}} \approx 3.2\text{ GHz}. \quad (39)$$

To evaluate the impact of the LED response on the intracavity pumping geometry, one should first consider the evolution of $|H(\omega)|^2$ at room temperature and at the optimum detuning δ_{opt} for different values of the input current J using Eqs. (26) and (28) [Figs. 7(a) and 7(b)]. Hence it is seen that for the electrical pumping case [Eq. (26)] with current densities in the range 10–20 A cm^{-2}, the peak frequency ω_P lies in the range 6–12 GHz and the cutoff frequency $\omega_{3\text{ dB}}$ is expected to be ~19 GHz [Fig. 7(b)]. Much larger values are predicted for the intracavity pumping geometry when using Eq. (28) ($\omega_{3\text{ dB}} \gg 400$ GHz). However, in this regime the modulation transfer function of the device is limited by the frequency response of the pumping LED, which has a cutoff frequency given by Eq. (34). Finally, we have to point out that the above-mentioned values are upper bounds since they do

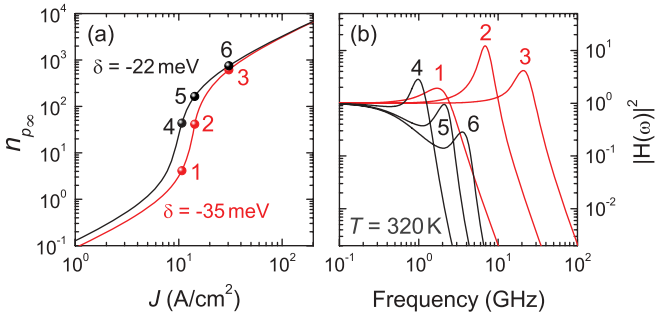

FIG. 7. (Color online) (a) Polariton condensate occupation number vs current density for the electrical (red line) and intracavity (black line) pumping geometries determined at 320 K and at the optimum detuning. (b) Frequency dependence ($\nu = \omega/2\pi$) of the square modulus of the modulation transfer function, $|H(\omega)|^2$. Each curve corresponds to one of the steady-state solutions indicated in Fig. 7(a).

not account, e.g., for possible electrical parasitic effects that could potentially affect the transmission line impedance.

IV. CONCLUSIONS

In summary, we have theoretically investigated some relevant electrical features of realistic III-nitride polariton LDs. First a formalism relying on coupled semiclassical Boltzmann equations adapted for an electrically driven exciton-polariton device was used to derive the evolution of the occupation number of the polariton ground state versus pump current density calculated for two pumping geometries: namely, the direct electrical and the intracavity optical pumping schemes. The corresponding condensation phase diagrams under electrical injection, i.e., plots of $J_{\rm thr}$ versus detuning and temperature, were also extracted. It led to the determination of the minimum threshold current density $J_{\rm thr,min}$ as a function of lattice temperature for the two pumping schemes. A $J_{\rm thr,min}$ value of $\sim$5 A cm^{-2} and 6 A cm^{-2} at RT has been derived for the direct electrical and the intracavity optical pumping geometries, respectively, which is close to previous estimates. Then a simplified rate equation modeling treatment was introduced to derive both steady-state and high-speed current modulation solutions. This simplified analysis made it possible to show that the carrier population which acts as a reservoir for the stimulated relaxation process, namely that of the excitons, gets clamped once it crosses the condensation threshold, which is a direct consequence of the similarities of the simplified rate equations with those describing conventional laser diodes. The analysis of the modulation transfer function, derived from the dynamical response of polariton LDs to a small modulation of the current above threshold, demonstrates the interesting potential of the direct electrical pumping scheme, since a cutoff frequency $\omega_{3\,\rm dB}$ up to $\sim$19 GHz is predicted, whereas for the intracavity optical pumping scheme, the cutoff frequency is shown to be limited by the frequency response of the pumping LED, for which $\omega_{3\,\rm dB} \approx 3.2$ GHz.

ACKNOWLEDGMENTS

This work was supported by the NCCR Quantum Photonics, research instrument of the Swiss National Science Foundation, by Grant No. 200020-113542, by the EU project Clermont4 of the FP7-People-ITN-2008 program under Grant No. FP7-235114, and by the EU FP7 IRSES project POLALAS. We are grateful to G. Cosendey for the realization of Fig. 1.

*Author to whom all correspondence should be addressed: raphael.butte@epfl.ch

[1] C. Weisbuch, M. Nishioka, A. Ishikawa, and Y. Arakawa, Phys. Rev. Lett. **69**, 3314 (1992).
[2] M. S. Skolnick, T. A. Fisher, and D. M. Whittaker, Semicond. Sci. Technol. **13**, 645 (1998).
[3] J. Kasprzak, M. Richard, S. Kundermann, A. Baas, P. Jeambrun, J. M. J. Keeling, F. M. Marchetti, M. H. Szymańska, R. André, J. L. Staehli, V. Savona, P. B. Littlewood, B. Deveaud, and Le Si Dang, Nature (London) **443**, 409 (2006).
[4] S. Christopoulos, G. Baldassarri Höger von Högersthal, A. Grundy, P. G. Lagoudakis, A. V. Kavokin, J. J. Baumberg, G. Christmann, R. Butté, E. Feltin, J.-F. Carlin, and N. Grandjean, Phys. Rev. Lett. **98**, 126405 (2007).
[5] G. Christmann, R. Butté, E. Feltin, J.-F. Carlin, and N. Grandjean, Appl. Phys. Lett. **93**, 051102 (2008).
[6] S. Kéna-Cohen and S. R. Forrest, Nat. Phot. **4**, 371 (2010).
[7] K. G. Lagoudakis, M. Wouters, M. Richard, A. Baas, I. Carusotto, R. André, L. S. Dang, and B. Deveaud-Plédran, Nat. Phys. **4**, 706 (2008).
[8] K. G. Lagoudakis, T. Ostatnický, A. V. Kavokin, Y. G. Rubo, R. André, and B. Deveaud-Plédran, Science **326**, 974 (2009).
[9] A. Amo, D. Sanvitto, F. P. Laussy, D. Ballarini, E. del Valle, M. D. Martin, A. Lemaître, J. Bloch, D. N. Krizhanovskii, M. S. Skolnick, C. Tejedor, and L. Viña, Nature (London) **457**, 291 (2009).
[10] A. Amo, J. Lefrère, S. Pigeon, C. Adrados, C. Ciuti, I. Carusotto, R. Houdré, E. Giacobino, and A. Bramati, Nat. Phys. **5**, 805 (2009).
[11] K. G. Lagoudakis, B. Pietka, M. Wouters, R. André, and B. Deveaud-Plédran, Phys. Rev. Lett. **105**, 120403 (2010).
[12] A. A. Khalifa, A. P. D. Love, D. N. Krizhanovskii, M. S. Skolnick, and J. S. Roberts, Appl. Phys. Lett. **92**, 061107 (2008); D. Bajoni, E. Semenova, A. Lemaître, S. Bouchoule, E. Wertz, P. Senellart, and J. Bloch, Phys. Rev. B **77**, 113303 (2008); S. I. Tsintzos, N. T. Pelekanos, G. Konstantinidis, Z. Hatzopoulos, and P. G. Savvidis, Nature (London) **453**, 372 (2008); S. I. Tsintzos, P. G. Savvidis, G. Deligeorgis, Z. Hatzopoulos, and N. T. Pelekanos, Appl. Phys. Lett. **94**, 071109 (2009).
[13] H. Mathieu, P. Lefebvre, and P. Christol, Phys. Rev. B **46**, 4092 (1992).
[14] M. Saba, C. Ciuti, J. Bloch, V. Thierry-Mieg, R. André, L. Si Dang, S. Kundermann, A. Mura, G. Bongiovanni, J. L. Staehli, and B. Deveaud, Nature (London) **414**, 731 (2001).
[15] R. Butté and N. Grandjean, Semicond. Sci. Technol. **26**, 014030 (2011).

[16]J. Levrat, R. Butté, E. Feltin, J.-F. Carlin, N. Grandjean, D. Solnyshkov, and G. Malpuech, Phys. Rev. B **84**, 199908(E) (2011). As mentioned in this erratum, the critical density for polariton condensation $n_{2D,crit}$ derived in J. Levrat *et al.*, *ibid.* **81**, 125305 (2010) (the present Ref. 43) was overestimated by a factor of 10 leading to the same error for the estimate of the threshold current density quoted in Ref. 15.

[17]A. Imamoğlu, R. J. Ram, S. Pau, and Y. Yamamoto, Phys. Rev. A **53**, 4250 (1996).

[18]See, e.g., L. A. Coldren and S. W. Corzine, *Diode Lasers and Photonic Integrated Circuits*, Chap. 2 (Wiley, New York, 1995).

[19]For a review, see I. A. Shelykh, A. V. Kavokin, Y. G. Rubo, T. C. H. Liew, and G. Malpuech, Semicond. Sci. Technol. **25**, 013001 (2010), and references therein.

[20]D. Solnyshkov, E. Petrolati, A. Di Carlo, and G. Malpuech, Appl. Phys. Lett. **94**, 011110 (2009).

[21]G. Christmann, R. Butté, E. Feltin, A. Mouti, P. A. Stadelmann, A. Castiglia, J.-F. Carlin, and N. Grandjean, Phys. Rev. B **77**, 085310 (2008).

[22]G. Christmann, R. Butté, E. Feltin, J.-F. Carlin, and N. Grandjean, Phys. Rev. B **73**, 153305 (2006).

[23]R. Butté, J. Levrat, G. Christmann, E. Feltin, J.-F. Carlin, and N. Grandjean, Phys. Rev. B **80**, 233301 (2009).

[24]M. Suzuki, J. Nishio, M. Onomura, and C. Hongo, J. Cryst. Growth **189/190**, 511 (1998).

[25]G. Cosendey, J.-F. Carlin, N. A. K. Kaufmann, R. Butté, and N. Grandjean, Appl. Phys. Lett. **98**, 181111 (2011).

[26]G. Christmann, D. Simeonov, R. Butté, E. Feltin, J.-F. Carlin, M. Mosca, and N. Grandjean, Appl. Phys. Lett. **89**, 261101 (2006).

[27]A. David, M. J. Grundmann, J. F. Kaeding, N. F. Gardner, T. G. Mihopoulos, and M. R. Krames, Appl. Phys. Lett. **92**, 053502 (2008).

[28]G. Malpuech, D. Solnyshkov, A. Di Carlo, and E. Petrolati, Bull. Officiel Propriété Industrielle **10/19**, 132 (2010), published by Institut National de la Propriété Industrielle, France.

[29]See R. Butté, G. Christmann, E. Feltin, A. Castiglia, J. Levrat, G. Cosendey, A. Altoukhov, J.-F. Carlin, and N. Grandjean, Proc. SPIE **7216**, 721619 (2009), and references therein.

[30]A. Castiglia, D. Simeonov, H.-J. Buehlmann, J.-F. Carlin, E. Feltin, J. Dorsaz, R. Butté, and N. Grandjean, Appl. Phys. Lett. **90**, 033514 (2007).

[31]T.-C. Lu, C.-C. Kao, H.-C. Kuo, G.-S. Huang, and S.-C. Wang, Appl. Phys. Lett. **92**, 141102 (2008); Y. Higuchi, K. Omae, H. Matsumura, and T. Mukai, Appl. Phys. Express **1**, 121102 (2008).

[32]S. Nakamura, G. Fasol, and S. J. Pearton, *The Blue Laser Diode: The Complete Story*, 2nd ed. (Springer, Berlin, 2000).

[33]V. Savona, L. C. Andreani, P. Schwendimann, and A. Quattropani, Solid State Commun. **93**, 733 (1995).

[34]H. A. McLeod, *Thin-Film Optical Filters*, 2nd ed. (Adam Hilger, Bristol, UK, 1986).

[35]H. Benisty, H. De Neve, and C. Weisbuch, IEEE J. Quantum Electron. **34**, 1612 (1998).

[36]The optical properties of SiO_2, TiO_2, and Si_3N_4 layers were determined by spectroscopic ellipsometry using thick layers grown on sapphire substrates.

[37]D. Brunner, H. Angerer, E. Bustarret, F. Freudenberg, R. Höpler, R. Dimitrov, O. Ambacher, and M. Stutzmann, J. Appl. Phys. **82**, 5090 (1997).

[38]J.-F. Carlin and M. Ilegems, Appl. Phys. Lett. **83**, 668 (2003).

[39]J.-F. Carlin, C. Zellweger, J. Dorsaz, S. Nicolay, G. Christmann, E. Feltin, R. Butté, and N. Grandjean, Phys. Status Solidi B **242**, 2326 (2005).

[40]M. J. Bergmann and H. C. Casey Jr., J. Appl. Phys. **84**, 1196 (1998).

[41]R. Schmidt, B. Rheinländer, M. Schubert, D. Spemann, T. Butz, J. Lenzner, E. M. Kaidashev, M. Lorenz, A. Rahm, H. C. Semmelhack, and M. Grundmann, Appl. Phys. Lett. **82**, 2260 (2003).

[42]J. Levrat, R. Butté, G. Christmann, E. Feltin, J.-F. Carlin, and N. Grandjean, Phys. Status Solidi C **6**, 2820 (2009).

[43]J. Levrat, R. Butté, E. Feltin, J.-F. Carlin, N. Grandjean, D. Solnyshkov, and G. Malpuech, Phys. Rev. B **81**, 125305 (2010).

[44]R. P. Leavitt and J. W. Little, Phys. Rev. B **42**, 11774 (1990).

[45]For this pumping geometry, taking into account the large number of quantum wells in QWs-2 and the high reflectivity of the bottom III-nitride DBR, it is a reasonable assumption to consider that all photons emitted downward from the pumping LED will be absorbed by QWs-2. For the sake of simplicity, a similar assumption has been made for photons emitted upward that would be perfectly reflected by the highly reflective top dielectric DBR and subsequently recycled by QWs-1 or more likely directly absorbed by QWs-2 (i.e., losses due, e.g., to the sidewall roughness and leaky modes have not been accounted for since their accurate estimate lies beyond the scope of this work).

[46]A. Castiglia (private communication). Such a linewidth is typical of optimized UV-violet LEDs emitting in the 390–420 nm range.

[47]A. V. Kavokin, J. J. Baumberg, G. Malpuech, and F. P. Laussy, *Microcavities* (Oxford University Press, Oxford, 2007), Appendix B.

[48]F. Tassone and Y. Yamamoto, Phys. Rev. B **59**, 10830 (1999).

[49]The value of τ_x is taken from the work of Narukawa and co-workers: Y. Narukawa, Y. Kawakami, S. Fujita, and S. Nakamura, Phys. Rev. B **59**, 10283 (1999), where it was shown that for state of the art InGaN QWs, localized and delocalized excitonic states exhibit nearly the same lifetime.

[50]W. G. Scheibenzuber, U. T. Schwarz, L. Sulmoni, J. Dorsaz, J.-F. Carlin, and N. Grandjean, J. Appl. Phys. **109**, 093106 (2011); W. G. Scheibenzuber, C. Hornuss, and U. T. Schwarz, Proc. SPIE **7953**, 79530K (2011). In those papers, it is shown that the charge carrier lifetime $\tau_{e\text{-}h}(N)$ in violet LDs amounts to 2–3 ns at threshold. Knowing that in the present case the polariton devices operate at lower carrier densities, a longer lifetime is expected according to the phenomenological ABC model accounting for radiative and nonradiative channels since $\frac{1}{\tau_{e\text{-}h}(N)} = A + BN + CN^2$. A $\tau_{e\text{-}h}$ value of 5 ns has therefore been chosen as a typical value.

[51]M. Suzuki, T. Uenoyama, and A. Yanase, Phys. Rev. B **52**, 8132 (1995).

[52]See, e.g., X. B. Zhang and B. Gil, in *Low-Dimensional Nitride Semiconductors*, edited by B. Gil (Oxford University Press, Oxford, 2002).

[53]R. Truell, C. Elbaum, and B. B. Chick, *Ultrasonic Methods in Solid State Physics* (Academic, New York, 1969).

[54]J. Kasprzak, D. D. Solnyshkov, R. André, Le Si Dang, and G. Malpuech, Phys. Rev. Lett. **101**, 146404 (2008).

[55]G. Malpuech, A. Kavokin, A. Di Carlo, and J. J. Baumberg, Phys. Rev. B **65**, 153310 (2002); A. Kavokin, G. Malpuech,

A. Di Carlo, and J. J. Baumberg, Phys. Status Solidi A **190**, 725 (2002).

[56]Because low J_{thr} values in the condensation phase diagram are essentially reported for negative δ values [cf. Figs. 4(a) and 4(b)], one should keep in mind that the present situation corresponds to a decrease of δ in absolute value.

[57]L. A. Coldren and S. W. Corzine, *Diode Lasers and Photonic Integrated Circuits* (Wiley, New York, 1995).

[58]By small perturbation it is meant that dynamic changes in the exciton and polariton populations away from their steady-state values are weak.

[59]For the sake of simplicity, one considers that the input parameters for the LED, namely the exciton formation rate W, the decay rate of the electron-hole plasma $\tau_{e\text{-}h}$, and the exciton lifetime τ_x, have the same values as defined earlier.